Acoustic Analogy for Oscillations Induced by Supersonic Flow over a Forward-Facing Nose Cavity

William Engblom*
Embry Riddle Aeronautical University, Daytona Beach, Florida, 32114

David Goldstein†
The University of Texas, Austin, Texas

The development of a spring-mass-damper acoustic analogy for oscillations induced by supersonic flow over a hemispherical nose with a cylindrical nose cavity is presented. The acoustic analogy is verified against computational fluid dynamics (CFD) simulations in which cavity oscillations develop due to sinusoidal freestream flow perturbations. The verification involves examination of parametric sensitivities including freestream perturbation noise frequency and amplitude, cavity length-to-diameter (L/D) ratio, freestream Mach number, and nose-to-cavity diameter ratio. Fluid mechanic and acoustic physical arguments are offered to explain the parametric sensitivities, as well as the onset of self-sustained oscillations for sufficiently deep cavities (i.e., oscillations without freestream flow perturbations). The CFD flow solver is validated for prediction of the onset of self-sustained oscillations against experimental data obtained in the Mach 4 Purdue Quiet Flow LudwiegTube (PQFLT).

Nomenclature

A	=	amplitude
b	=	dissipation coefficient
c	=	speed of sound
D	=	cavity diameter
f	=	frequency
G	=	amplification
k	=	stiffness
L	=	cavity length (depth)
L*	=	distance from bow shock to cavity basewall along centerline
m	=	mass
M	=	Mach number
p	=	static pressure
R	=	radiation resistance coefficient
t	=	time
T	=	static temperature
u	=	axial velocity
wn	=	wave number
x	=	spring deformation
X	=	inductance coefficient
Z	=	impedance
δ	=	shock standoff distance
ρ	=	density

Subscripts

c	=	corrected
o	=	stagnation conditions downstream of bow shock
opt	=	optimal
n	=	nose
s	=	static equilibrium
∞	=	freestream

I. Introduction

Hypersonic vehicles such as hypervelocity projectiles, interceptor missiles, re-entry vehicles, and hypersonic aircraft are designed to withstand severe heat loads. Maximum aerodynamic heating and potential for material ablation is typically most critical at the nose tips and leading-edges. Consequently, it is desirable to consider new active and passive techniques to reduce tip heating rates and delay or eliminate onset of ablation.

---

* Associate Professor, Mechanical Eng. Dept., Daytona Beach, Associate Fellow AIAA (engbl7de@erau.edu)
† Professor, Aerospace Engineering and Engineering Mechanics Dept., Austin, Senior Member AIAA

One such technique that appears to have promise is to shape the nose using a forward-facing cavity. Hartmann [Ref. 1] established that placing a forward-facing cavity in a nose can produce intense pressure oscillations at a discrete frequency when placed within a supersonic flow (i.e., the Hartmann whistle). Engblom et al [Ref 2] showed numerically and experimentally that only cavities with a sufficient depth-to-diameter ratio will self-sustain intense pressure oscillations, but oscillations within more shallow cavities can be driven by freestream noise. Numerical simulations by Engblom and Goldstein [Ref. 3] also indicate that strong resonance induces a "cooling effect", resulting in substantially reduced peak nose-tip heat transfer rates. The reduced peak heat transfer is thought to be related to i) movement of stagnation point and associated redistribution of heat transfer input, ii) boundary layer thickening due to oscillations, and iii) reduction of stagnation temperature of gas reaching cavity due to bow shock motion. An experimental investigation of the potential to delay ablation onset by Silton and Goldstein [Ref. 4] using hemispherical ice test articles in a Mach 5 tunnel did suggest moderate improvement due to addition of a cylindrical cavity.

II. Objective

A fundamental understanding of the fluid physics involved is desired to address potential applications for the resonating forward-facing cavity in supersonic flow, including for the potential heat transfer reduction effect. The main goal of this work is to develop, and verify against CFD, an acoustic analogy which adequately models the unsteady behavior of hypersonic flow over a nose with cavity, including the sensitivity to key geometric parameters and flight conditions.

A secondary goal is to examine the onset of self-sustained cavity oscillations, first observed numerically [Ref. 2], and then recently reported experimentally by Juliano, et al [Ref. 5] for Mach 4 flow over hemispherical test articles with sufficiently deep cylindrical cavities. The latter study was conducted in the Purdue Quiet Flow Ludwieg Tube (PQFLT) to effectively remove tunnel noise effects. In the present study, the CFD solver is validated by computing unsteady Navier-Stokes solutions in a quiescent freestream, for direct comparison with experimental results.

III. Methodology

A. Parametric Study Description

The run condition and geometric parameter space to be evaluated with both CFD and an acoustic model analog are provided in Table 1. The freestream static conditions (p_∞ = 4700Pa, T_∞=64K) are chosen from the Supersonic Blowdown Facility at the University of Texas Pickle Research Center, and are the same for all cases. The baseline geometry, shown in Fig 1a, has a one-inch cavity diameter, two-inch nose diameter, and a cavity depth of 0.75 inches (i.e., L/D=0.75, D_n/D=2.0). The baseline run conditions include a Mach 5 freestream and oscillations are driven by input of ±1% amplitude sinusoidal variations in freestream pressure and density (isothermal noise). The parameter space is evaluated by varying one of the four parameters in Table 1, while maintaining all other parameters fixed. It should be noted that, for each point in the parameter space, the noise input frequency is varied such that the frequency which produces the strongest pressure oscillations within the cavity is captured. The range of L/D ratio is chosen to avoid self-sustaining oscillations which occur around L/D=1.2 for these conditions based on previous numerical and experimental evaluations [Ref. 2]. The two-block, structured, axisymmetric grids used for these evaluations are shown in Fig. 1. The baseline grid contains IxJxK blocks of size 41x41x2 (cavity) and 81x101x2 (outside cavity), and 5° wedge for axisymmetric computations.

Table 1: Parameter space for CFD and acoustic analogy evaluations

L/D	A (%)	M_∞	D_n/D
0.25	±0.5	3.0	**2.0**
0.75	**±1.0**	**5.0**	4.0
1.1	±2.0	7.0	8.0
	±3.0	9.0	16.0

*baseline conditions are in boldface

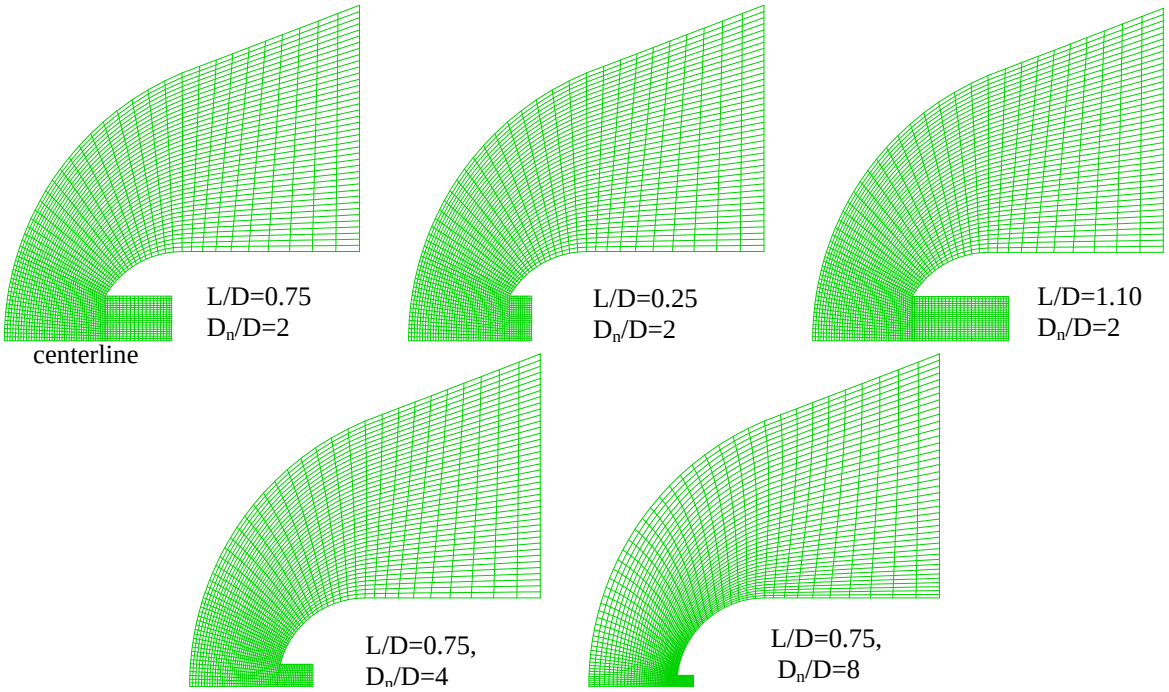

Figure 1: Hemispherical nose plus cylindrical cavity geometries and grids
(every other grid point removed)

B. CFD Solver

The TESTBED flow solver uses a density-based, finite-volume, cell-centered, multi-block structured-grid formulation. A brief discussion of code methodology and validation can be found in Engblom [Ref. 6]. In the present study, the time-dependent Navier-Stokes equations are solved for air as a thermally and calorically perfect gas. The inviscid fluxes are treated using the Van Leer flux vector splitting scheme. Second-order spatial accuracy is achieved by MUSCL extrapolation. Using a pressure-based switching function, the second-order spatial fluxes are reduced to first-order in the vicinity of shock waves automatically in regions with large 2^{nd}-order pressure gradients. Viscous fluxes are evaluated with central differencing. Second-order accurate time-marching is achieved using a lower-upper symmetric Gauss-Seidel (SGS) implicit scheme, with sufficient subiterations (typically 10) to converge the L_2-norm of the solution change at each time step to within a tolerance of 1e-5.

C. Validation of Flow Solver using PQFLT Data

Prior to evaluating the parameter space identified in Table 1, the flow solver was validated against a recently available set of experimental data. Juliano et al [Ref. 5] investigated the response of cylindrical nose cavities in a hemisphere cylinder body in the Mach 4 Purdue Quiet Ludwieg Tube Facility (PQFLT). The cavity and nose diameters are 0.375 and 0.750 inches, respectively (see Fig. 2). This geometry is equivalent to a half-scale version of the baseline geometry described in the previous section. By systematically varying the cavity depth, they were able to clearly determine the onset of self-sustained oscillations. The freestream noise levels in the PQFLT are roughly 0.006% rms, and so only register weak oscillations in noise-driven, shallow cavities. A sharp increase in oscillation strength occurs at L/D=1.2, demonstrating the onset of the self-sustained oscillation regime. Although this regime has been identified from data obtained in the Mach 5 blowdown facility at the University of Texas [Ref. 2], the noise levels of roughly 2% obscure the sharp onset which occurs.

The TESTBED flow solver is used to emulate the PQFLT tests. In these simulations, a quiescent freestream is applied (i.e., not noise driven) to emulate the PQFLT. Mach 4 flow corresponding to the PQFLT experiments (p_∞=

363.1 Pa, T_∞= 70.7 K) is simulated in conjunction with range of cavity depths (or L/D ratios with fixed diameter) from the PQFLT experiments (L/Ds from 0.5 to 3.0). Figures 3a and 3b show spectral content of self-sustained oscillations from the experiment [Ref. 5] and current CFD evaluation. Resonance at the primary organ-pipe mode is found, as expected. Power at higher harmonic frequencies is also apparent, although two orders-of-magnitude weaker in the CFD results. The asymptotic behavior of peak power levels at large cavity depths is consistent between the CFD and PQFLT experimental data. The peak power levels are expected to agree well, so the source of the mismatch on the peak power levels is likely attributed to an error in the spectral analysis.

Figure 4a shows the numerical predictions for the variation of oscillation strength with cavity depth, and a predicted onset of self-sustained oscillations at L/D=1.2. The strength of the oscillations grows rapidly with increased cavity depth, reaching rms levels of over 30% of the mean pressure in cavity base. These paek levels are consistent with those found in previous numerical and experimental analysis at Mach 5 [Ref. 2].

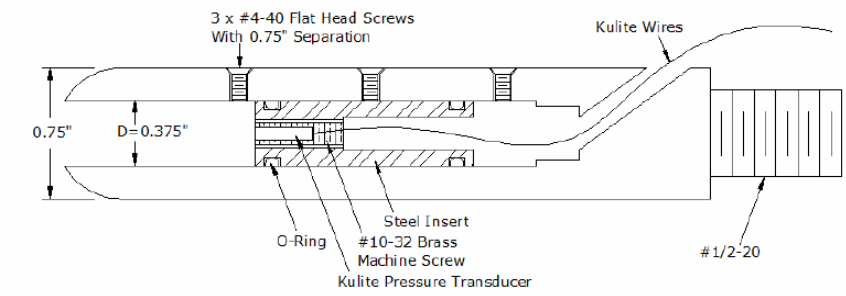

Figure 2. Test article for PQFLT evaluation [Ref. 5]

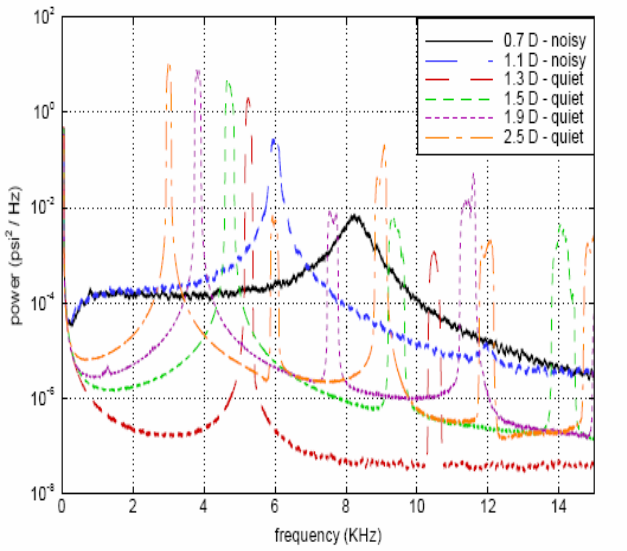

Figure 3a. Power spectra of self-sustained oscillations for several cavity depths (PQFLT) [Ref. 5]

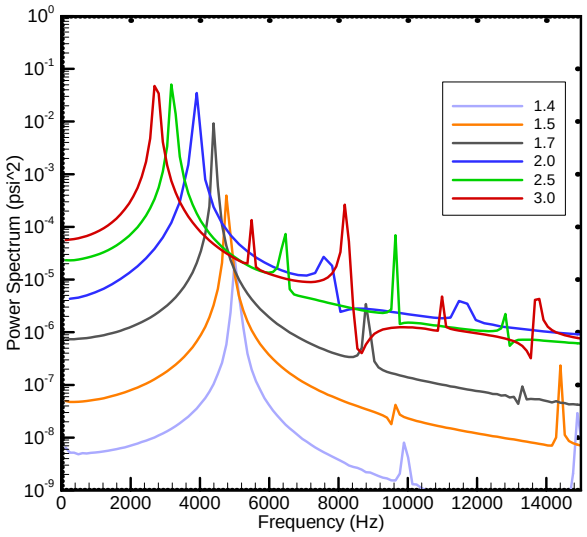

Figure 3b. Power spectra for self-sustained oscillations for several cavity depths (CFD)

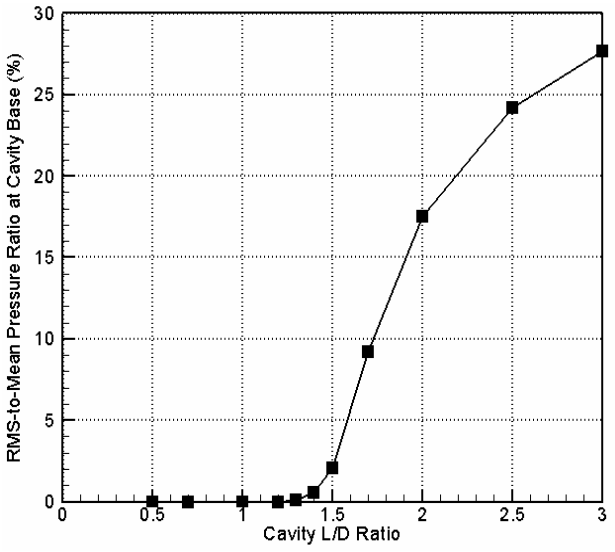

Figure 4a. Normalized rms base pressure oscillations vs. cavity depth (CFD)

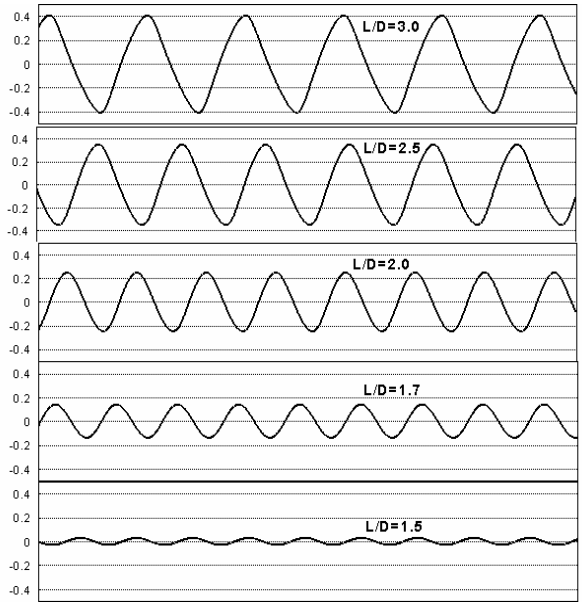

Figure 4b. Basewall pressure history normalized by mean pressure (CFD)

Figure 4b illustrates how the self-sustained oscillations manifest themselves in terms of near-sinusoidal base pressure oscillations at the primary mode. A more saw-tooth shape signal begins to develop at large cavity lengths, as the bow shock oscillations become restricted by limited shock standoff distance. Base pressure varies by ±40% for L/D=3.0.

It is found that the choice of flux limiter has a significant effect on the numerical results. Initial attempts using a min-mod limiter rather than the pressure-switch based limiter, resulted in delayed onset of self-sustained oscillations. Although laminar viscous effects are included, initial runs without viscous effects showed negligible change to the results herein.

D. Acoustic Analogy Description

It has been suggested [Ref. 2] that the response of a relatively shallow cavity to inflow noise (e.g., pressure fluctuations) is analogous to the response of damped harmonic oscillator to a forcing function. It has been shown that shallow cavities (e.g., L/D < 1.2 at Mach 5) require the presence of inflow noise containing energy near the primary mode (or organ-pipe) frequency in order to resonate. This primary mode frequency [Eqn. 1] is evaluated from the speed of sound of gas within cavity divided by the wavelength of four times the distance from bow shock at cavity mouth to cavity basewall (i.e., cavity length plus mean shock standoff). The speed-of-sound can be approximated as the freestream stagnation value since the flow within the cavity is relatively stagnant.

$$f = c_o / \lambda \quad where \;\; \lambda = 4(L + \delta) \tag{1}$$

It has been shown [Ref. 2] that the strength of the pressure oscillations for a given cavity configuration is nearly proportional to the strength of the pressure oscillations in the freestream. That is, the amplification (G), defined in Eqn. 2, is nearly constant for a given cavity configuration and mean freestream conditions. A linear spring-mass-damper system also possesses this characteristic.

$$G = \frac{p_{basewall,rms}}{p_{\infty,rms}} \tag{2}$$

We choose to create an acoustic analog using the mechanical lumped elements of mass, stiffness, and damping. Acoustic analogs assume small disturbances to the mean flow, and lumped elements assume a quasi-static behavior for the fluid element. The Helmholtz resonator (Fig. 5) radiating noise into a confined duct is the most similar, classical acoustic analog to the current Hartmann whistle device. In the Helmholtz resonator, the source of the oscillations are acoustic perturbations (noise input) reaching the resonator (e.g., when one blows air across the inlet creating periodic vortex shedding). The neck region is a mass element since it accelerates uniformly up-and-down during resonance (i.e., vibrates as a rigid body). The chamber is a stiffness element since the pressure is quasi-static (i.e., spatially uniform) as it oscillates in time. Noise is radiated by the vibrating mass element to the farfield (infinite medium), and is known as piston radiation, which represents the damping element (also termed radiation resistance). Morse and Ingard [Ref. 6] conclude that if the mass radiates within a confined finite medium, this dissipation is not present and the main dissipation is likely due to viscous losses.

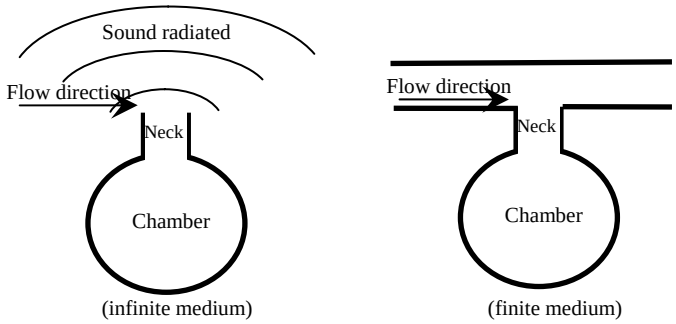

Figure 5. Helmholtz Resonator

Supersonic flow over a forward-facing cavity (or Hartmann whistle) can be modeled somewhat analogously. The small disturbance assumption can be satisfied for weakly-oscillating, noise-driven cavities; however, this condition is violated for deep cavities which naturally develop strong self-sustained pressure oscillations. The cylindrical cavity resembles a Helmholtz resonator except that there is no longer a distinct boundary between the neck (mass) and chamber (stiffness) regions. Also, the bow shock becomes a kind of radiation reflector. Since we know the natural frequency is well-predicted by Eqn. 2, the relationship between the mass and stiffness for a harmonic oscillator can be utilized [Eqn. 3]. We need only obtain either the mass or stiffness.

$$f = \frac{1}{2\pi}\sqrt{\frac{k}{m}} \tag{3}$$

Figure 6 illustrates the pressure contours and streamlines at two realizations (snapshots in time) for the baseline Mach 5 case in Table 1, except with ±3% amplitude sinusoidal freestream noise input at a frequency of 3450 Hz. This two-part figure is representative of the cavity purge and cavity fill modes within one cycle, respectively. When the freestream pressure increases, the stagnation pressure downstream of the bow shock increases and tends to cause cavity inflow and an increase in cavity pressure. When the freestream pressure decreases, the stagnation pressure downstream of the bow shock decreases and tends to permit the cavity flow to purge and a decrease in cavity pressure. The time lag between the pressure changes at the bow shock and within the cavity can lead to dramatic unsteady response (as shown here).

Figure 7 illustrates the "acoustic" pressure distributions (i.e., deviation from mean stagnation pressure behind bow shock) along the centerline of the flowfield at 20 realizations during one cycle after the flow has reached a pseudo-steady state. These distributions are representative, and are generated for the baseline Mach 5 case in Table 1, except with ±3% amplitude sinusoidal noise input. Clearly, the pressure distributions within the cavity resemble quarter since wave distributions at each realization.

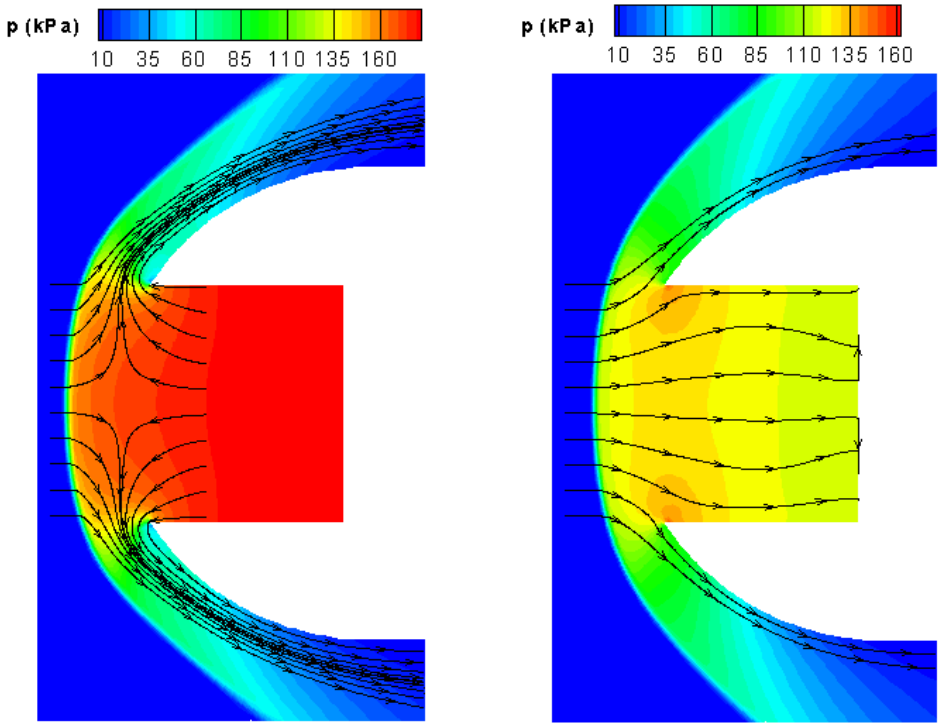

Figure 6. Pressure contours and streamlines for two snapshots during cycle: fill (right); purge (left) (note that color bars are different)

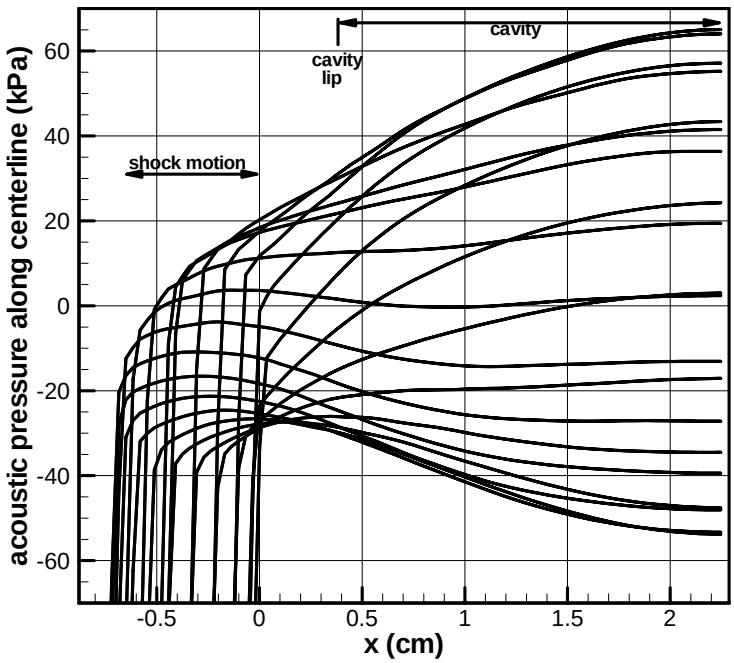

Figure 7. CFD-generated centerline pressure distributions for 20 realizations of one cycle (M=5, L/D=0.75, ±3% noise amplitude)

In order to be treated as a lumped mass element, a region of should be accelerating uniformly. Since the pressure distributions within the cavity involve primarily 1-D axial variations (see Fig. 6) and viscous effects are secondary, it is appropriate to consider the substantial derivative in the 1-D Euler equations to represent the total acceleration at a given point [Eqn. 4]. If the pressure gradient were constant, the acceleration would be uniform if we neglected the effect of density variations.

$$\frac{Du}{Dt} = -\frac{1}{\rho}\frac{\partial p}{\partial x} \tag{4}$$

But since the axial pressure gradient within the cavity is not uniform, we are forced to make an approximation. We obtain an average axial acceleration for the fluid within the cavity using a pressure gradient along the cavity, and assume that the cavity fluid accelerates uniformly as a lumped mass element. Eqn 5 describes the mass (per unit cavity cross-sectional area).

$$m = \rho_o L \tag{5}$$

Since the pressure distributions are typically monotonic in Figure 7, this is a reasonable approximation. The pressure gradients near the cavity basewall tend towards zero in each realization (the basewall is the anti-node in this quarter wave resonator). Since the fluid near the basewall has spatially uniform pressure, this region can be treated as a lumped spring element, per the chamber in a Helmholtz resonator. The pressure force applied to the mass element at the cavity mouth is assumed to be the stagnation pressure just downstream of the bow shock, which will vary according the amplitude and frequency of the freestream noise [Eqn. 6]. The effect of bow shock motion on the stagnation pressure is neglected.

$$p_{input} = p_o\,(1 + A\sin(2\pi f t)) \tag{6}$$

The pressure at the base wall will be calculated based on the spring constant obtained from Eqn. 3, and the current elastic deformation of the spring (x) from its equilibrium position (x=0). The x position is also the distance moved by the mass element from its original unperturbed postion. This equilibrium position requires that the spring force per unit area equals the input pressure, without freestream perturbations ($p_{\text{input}} = p_{\text{basewall}}$).

$$\begin{aligned} k &= (2\pi f)^2 m \\ p_{basewall} &= k(x - x_s) \quad where \quad x_s = p_{input}/k \end{aligned} \tag{7}$$

The primary dissipation mechanism is assumed to be associated with the radiation of acoustic energy from a vibrating cavity mass element from the cavity mouth and towards the farfield, as with the Helmholtz resonator. CFD simulations have shown that oscillation strength is negligibly affected by viscous and wall heat transfer effects for the nose-cavity geometry and operating conditions investigated here [Ref. 7].

The classical analytical treatment of a vibrating mass element which radiates within a surrounding structure (baffle) to a semi-infinite domain is known as baffled-piston radiation [Ref. 6], shown schematically in Figure 8. An analytical expression for the complex pressure field is calculated by integrating the effect of simple sources representing the vibrating surface. The complex impedance at the piston face, Z_p, is obtained by dividing the pressure there by the piston velocity amplitude. The real portion (R) represents the radiation resistance, and can be related to the dissipation coefficient (b) in a mechanical system [Eqn. 8]. The imaginary portion (X) represents the acoustic inductance which can be related to an additional mass element (Δm) to be added to the cavity mass in the mechanical system [Eqn. 8]. Note that the stagnation conditions behind the bow shock are used to represent the farfield conditions needed in these relations. Figure 9 provides the analytical values for these two components as function of the acoustic wave number (wn). At very low frequencies the resistance coefficient tends towards zero as no acoustic energy is transmitted by the mechanism. At very high frequencies the resistance coefficent tends towards unity.

$$b = Z_o R(wn) \quad and \quad \Delta m = \rho_o X(wn)/(2\pi f)$$
$$where \quad Z_o = \rho_o c_o \quad and \quad wn = 2\pi D f / c_o \tag{8}$$

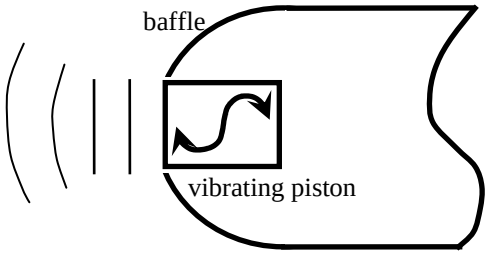

Figure 8. Baffled-piston radiating into a semi-infinite medium

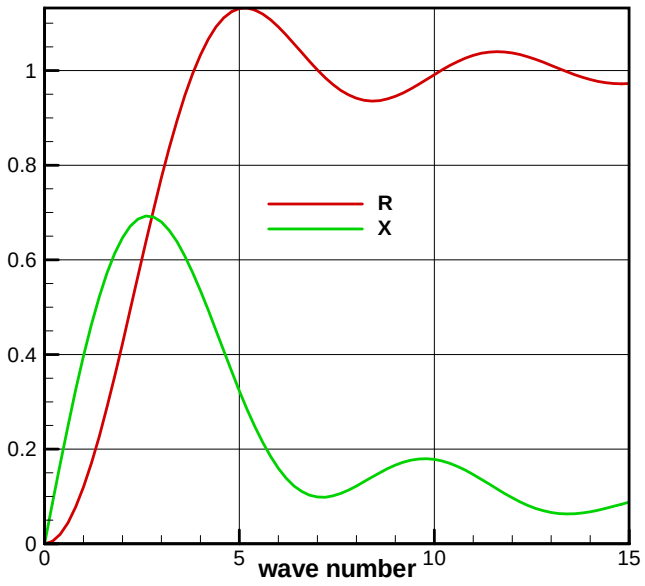

Figure 9. Baffled-piston radiation resistance and inductance

Unfortunately, these analytical baffled piston relations cannot be used in the present analog without additional modification due to effect of the bow shock as a reflector. It is easy to imagine that much of the acoustic energy radiating towards the bow shock is reflected back towards the cavity mouth by the bow shock, which acts as a constant pressure (zero acoustic pressure) boundary that will reflect and invert acoustic waves without upstream noise transmission. The approach proposed here is to super-impose the effect of an image-piston position 2δ from the original baffled piston face located at the cavity mouth (see Figure 10). The image piston is oscillating 180° out-of-phase with the baffled piston to ensure a constant pressure boundary at the bow shock. An analytical expression for the decay of the pressure fluctuations along the centerline of a baffled piston gives an approximation to the magnitude of the pressure fluctuations which will reach the original piston face [Ref. 6], and potentially reduce the radiation resistance and inductance (i.e., reinforce the oscillations). The modified formula for the dissipation coefficient is given as Eqn 9. Note that the dissipation appropriately tends to zero as the bow shock standoff distance approaches zero.

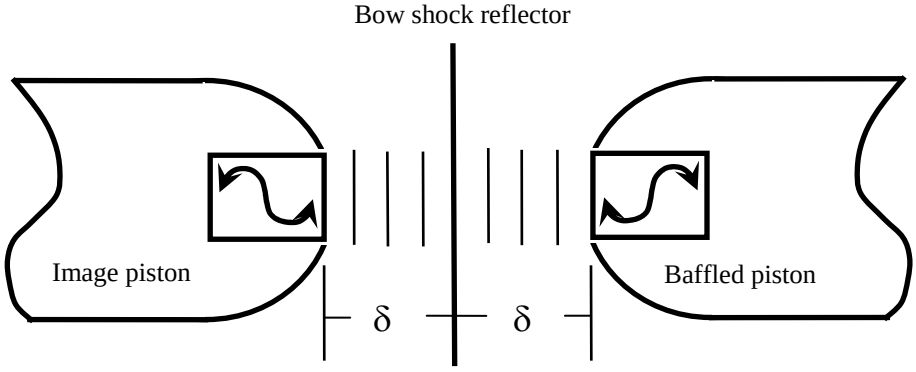

Figure 10. Schematic of baffled pistons

$$b = Z_o R\left(1 - \frac{1}{\sqrt{1 + 4\delta / D}}\right) \tag{9}$$

In summary, a spring-mass-damper (SMD) model has been formulated based on combination of consideration of classical acoustic analogies and fluid dynamic observations. A schematic is provided below in Fig 11. The 2nd order linear system which described the motion of the mass results in the two first order ODEs provided in Eqn. 10. Although closed form analytical solutions may be obtained, these equations are integrated forward in time using a 4th-order accurate Runge-Kutta integration scheme to examine both transient and pseudo-steady oscillatory behavior.

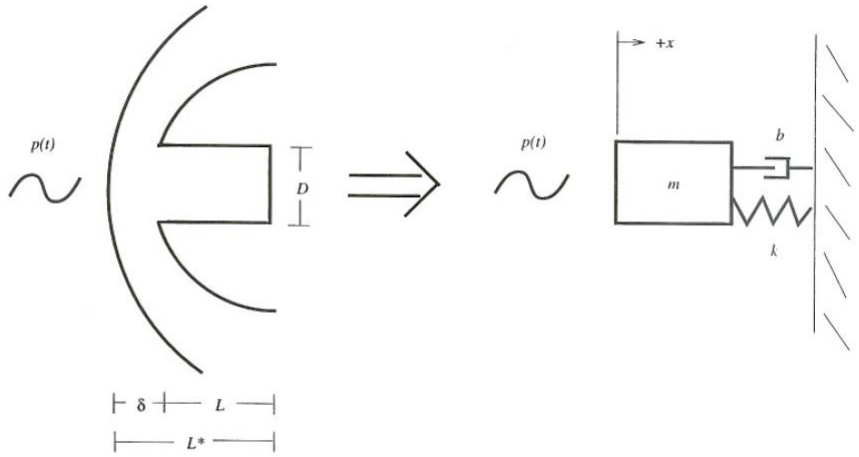

Figure 11. Schematic of Spring-Mass-Damper Analog

$$\begin{aligned} \dot{x} &= u \\ \dot{u} &= (p_{input} - p_{basewall} - b\dot{u})/(m + \Delta m) \end{aligned} \tag{10}$$

IV. Results

Now that we have verified CFD code results against PQFLT experiments, and developed a SMD acoustic analogy, we explicitly examine the flow physics associated with resonance mechanisms with both the CFD and the SMD model. A parametric study is conducted to investigate the sensitivity of the strength of pressure oscillations within a forward-facing cylindrical cavity to each of the following parameters independently, as described in Table 1: i) noise frequency, ii) noise amplitude, iii) cavity depth, iv) freestream Mach number, and v) nose-to-cavity diameter ratio. In all cases examined, numerical resonance is simulated by input of sinusoidal freestream noise at a discrete frequency. Results from the CFD and the SMD model are directly compared. The metric for comparison is the amplification or gain (G) of the freestream noise within the cavity, as defined in Eqn. 2.

The baseline case is a medium-depth cavity (L/D=0.75) with a sharp lip (as illustrated in Fig. 1). The baseline inflow noise profile includes a sinusoidal variation with peak-to-peak amplitude of pressure and density of ±1% (i.e., isothermal freestream noise, as defined in Eqn. 6. The mean static flow conditions correspond to those for the test section of the Mach 5 blowdown facility at the University of Texas (i.e., M_∞=5.0, T_∞= 64K, p_∞=4702 Pa).

A. Sensitivity of Amplification to Noise Frequency

Figure 12 shows the variation in G with freestream noise frequency (f) for the baseline case using both the Navier-Stokes CFD solver and the SMD acoustic analog. In each case sufficient cycles are computed until repeatable cyclic behavior is obtained (i.e., pseudo-steady). There is good agreement for the peak amplitude and roll-off rates between the CFD and SMD model predictions. The frequency for optimal amplification is roughly 200 Hz or ~5% lower in the CFD than for the SMD model. The source of this discrepancy is unknown. The CFD curve is also approximately 20% "wider" suggesting the cavity behavior deviates from linear oscillator behavior. Note that the SMD model contains no adjustable constants.

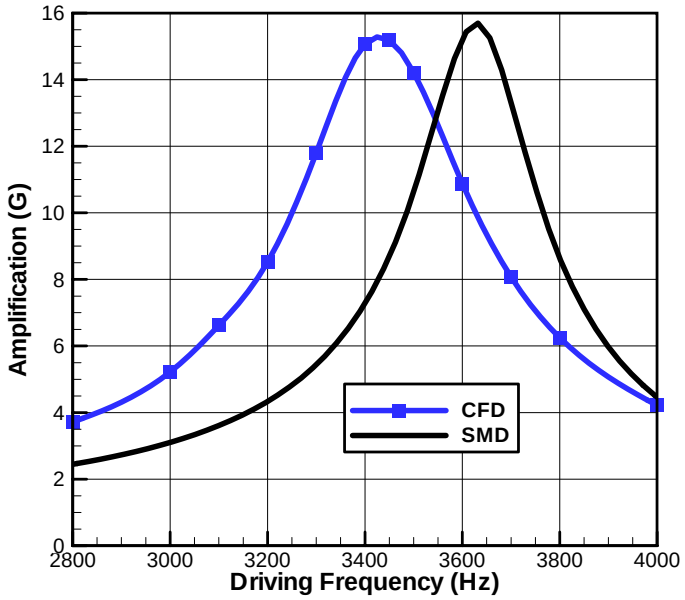

Figure 12. Amplification versus freestream noise frequency

B. Sensitivity of Amplification to Noise Amplitude

Figure 13 shows the variation in G with freestream noise amplitude for the baseline L/D=0.75 cavity configuration. The sinusoidal freestream noise input amplitude varies from ±0.5% to ±3%. The SMD model predicts constant amplification, as expected for linear harmonic oscillator. The CFD also indicates this linear behavior for smallest amplitudes, but the amplification begins to drop for large noise amplitudes. This occurs because bow shock motion is spatially limited by the presence of the cavity mouth. The bow shock actually reaches the cavity mouth and stops for a short time when the oscillations are sufficiently strong. This produces the shark-tooth like pressure signal of Figure 4b (L/D=3) and is interpreted as a saturation of the oscillation strength.

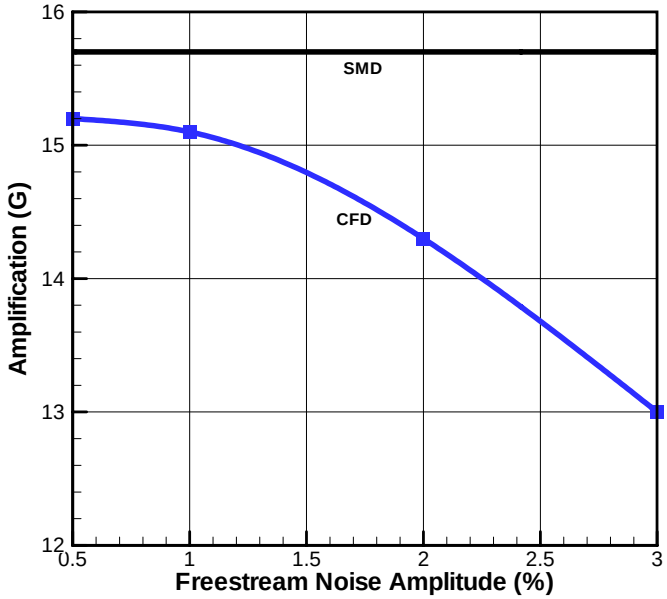

Figure 13. Amplification versus freestream noise amplitude

C. Sensitivity of Amplification to Cavity Depth

Figure 14 displays the variation in G with cavity depth (i.e., for L/D=0.25, 0.75, 1.10) for Mach 5 freestream and a freestream noise amplitude of ±1%, for both the CFD solver and SMD analog. For the CFD, typically three or four simulations are performed for each cavity depth to isolate the frequency which provides the optimal amplification (f_{opt}). The peaks of amplification versus freestream noise frequency become higher and sharper as cavity depth increases. The increase of normalized amplification roll-off, $|dG/d(f/f_{opt})|$, with amplification is consistent with a damped harmonic oscillator. There is excellent agreement between the SMD analog and CFD for the peak amplification. Again, the SMD results produce roughly a 5-8% larger optimal frequency, which is possibly due to nature of freestream noise implementation, as discussed earlier.

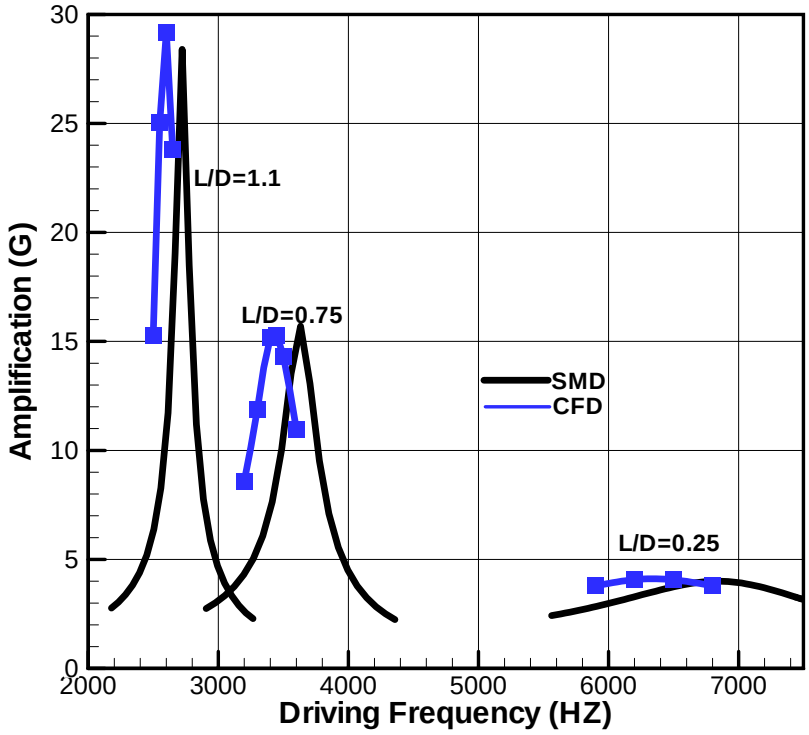

Figure 14. Amplification versus cavity depth

Figure 15 includes basewall pressure histories from start-up for the L/D=0.25 and 0.75 cases, driven at f_{opt} identified above with ±2% noise amplitude for both the CFD solver and SMD analog. Note the excellent agreement between these time histories between the CFD and SMD analog, for both cavities. Although the curves don't match, due to the different frequencies involved, the pressure oscillations grow at similar rates. The CFD predicts a slightly faster rate of increase in oscillation strength, and is quicker to completely level-off. The SMD model predicts the gradual asymptotic increase in oscillation strength to be expected from a linear harmonic oscillator. The deeper cavity takes longer to reach pseudo-steady behavior due to smaller level of dissipation present in the system.

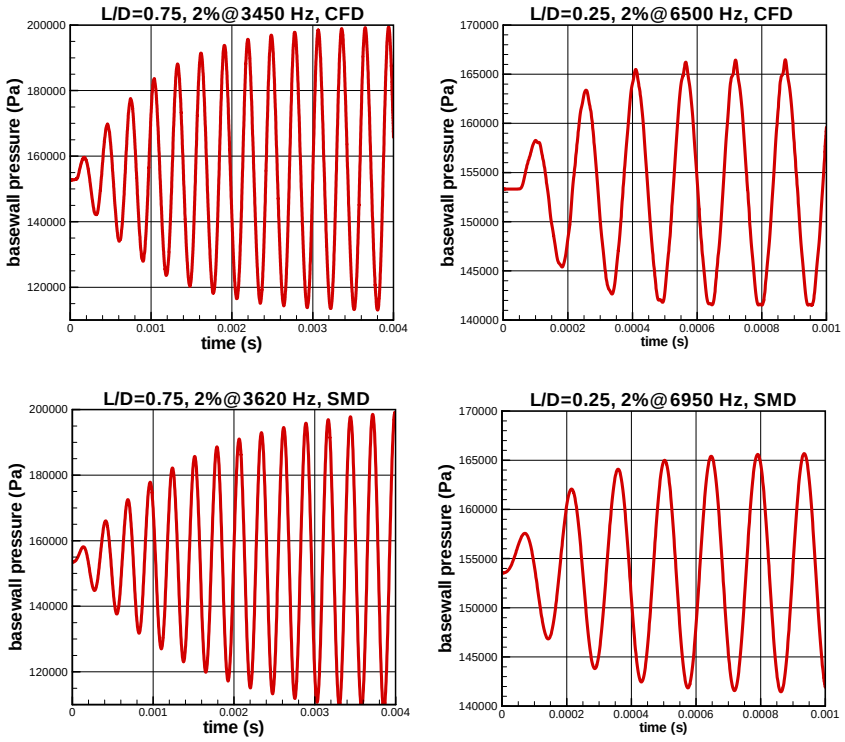

Figure 15. Basewall pressure histories for two cavity depths using CFD solver and SMD analog

Sensitivity of Amplification to Freestream Mach number

Figure 16 shows the sensitivity in G with respect to freestream Mach number. For each case, the baseline L/D=0.75 geometry is used along with a ±2% amplitude noise input. Again, for the CFD, typically three or four separate simulations are performed for each M_∞ to isolate the frequency which provides the optimal amplification (f_{opt}). Adiabatic no-slip wall conditions are applied to nose-cavity walls for all CFD simulations. Both the CFD and SMD analog show an asymptotic increase in amplification with M_∞. However, the SMD analog is unable to capture the large drop in amplification for the lower Mach 3 case.

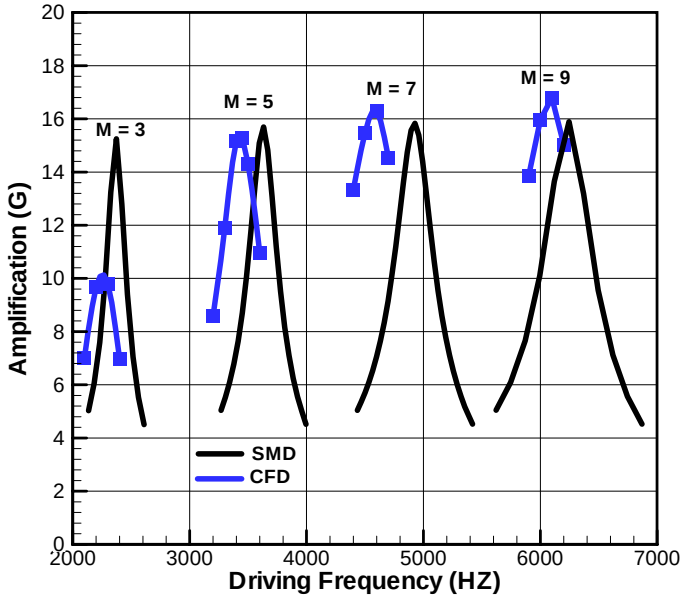

Figure 16. Amplification versus freestream Mach number

The SMD predicts the amplification should drop at lower M_∞ since the bow shock standoff distance increases and reduces the benefit posed by bow shock reflection of acoustic energy. However, the lower oscillation frequencies associated with lower M_∞ also reduce the radiation resistance, R, according to Fig. 9. Consequently, the SMD analog predicts only a minor net drop in amplification at $M_\infty = 3$.

D. Sensitivity of Amplification to Nose-to-Cavity Diameter

Figure 17 illustrates spline-fitted results for the optimum amplification and related optimal driving frequency for three different D_n/D ratios. The cavity geometry maintains an L/D=0.75, and baseline Mach 5 flow conditions. The CFD results indicate a highly non-linear variation with D_n/D, reaching a peak value at D_n/D =4, followed by gradual decrease in amplification for larger nose diameters. The SMD model results show little sensitivity in the amplification to D_n/D. There is clearly significant physics missing from the SMD model.

An explanation for the maximum in the CFD results involves the effect of radial convection currents near the cavity mouth. Figure 18 shows Mach contours for non-perturbed Mach 5 flows over the D_n/D =2 and 4 geometries. It is observed that these currents are much stronger in the D_n/D =2 case, due to the close proximity of the bow shock, reaching about Mach 0.5 along an axial line between the cavity lip and bow shock. As D_n/D increases, these convection effects weaken and decrease the acoustic wave speeds in the radial direction, thereby increasing the level of acoustic energy transmitted between the cavity mouth and bow shock, and hence the amplification. This effect competes with an asymptotic decline in amplification as D_n/D increases to be discussed below, and leads to a maximum.

The asymptotic decline in amplification in the CFD results is expected. As the cavity shrinks in scale on the same nose body, the cavity dimensions become small relative to the characteristic quarter wavelength (L^*). Consequently, the cavity gas approaches a quasi-static condition and the cavity is unable to maintain a significant pressure gradient. The mass within the cavity effectively becomes a spring. The original SMD model assumes the flow within the cavity behaves as a mass and spring. Consequently, a correction to the SMD model is proposed to scale the cavity mass with $(L/L^*)^2$ in Eqn. 11, along with a correction to dissipation to calibrate the baseline case result. A similar asymptotic decrease in amplification to that from the CFD is recovered by this adjustment, referred to as SMD-2. Although not shown, SMD-2 produces similar results for the all the other parameters discussed with exception of L/D=0.25 case for which the amplification is under predicted by 50%. The low M_∞ sensitivity results are also improved with SMD-2.

Figure 17 also shows that the optimal frequency deviates dramatically between the SMD and CFD results at large D_n/D. The SMD model assumes the organ-pipe frequency is based on L^*, but the CFD predicts much higher optimal frequencies at large D_n/D. At large D_n/D, the flow within the characteristic frequency would be better described by an organ-pipe mode based on the cavity length, rather than L^*, since the influence of the bow shock has effectively disappeared; it is simply too far away from the cavity mouth.

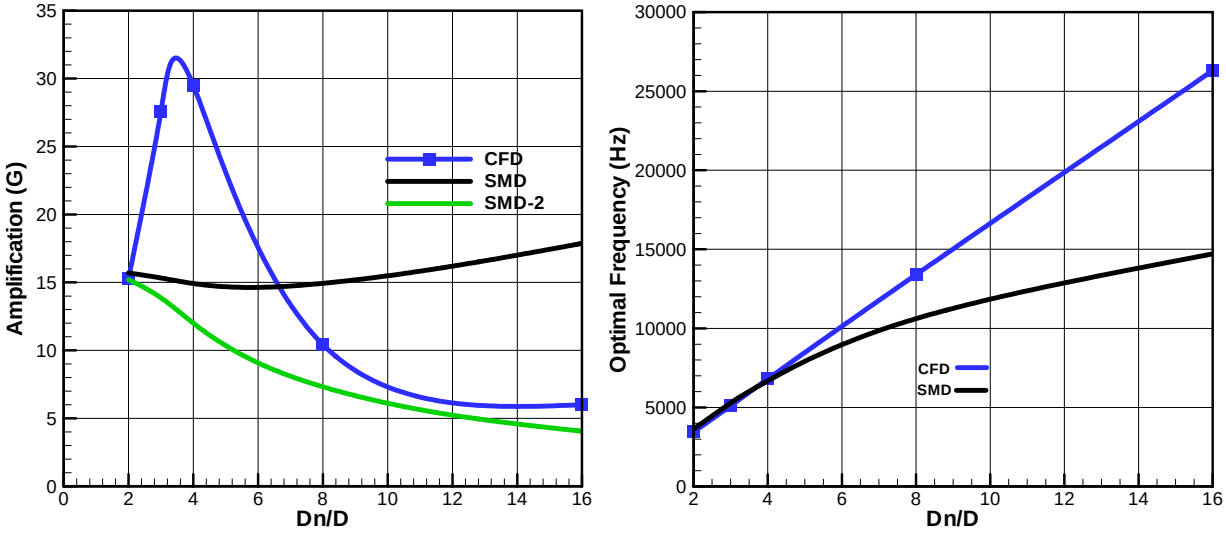

Figure 17. Amplification and optimal frequency versus nose-to-cavity diameter ratio

$$m_c = m \cdot (L / L^*)^2$$
$$b_c = 0.68\, b \tag{11}$$

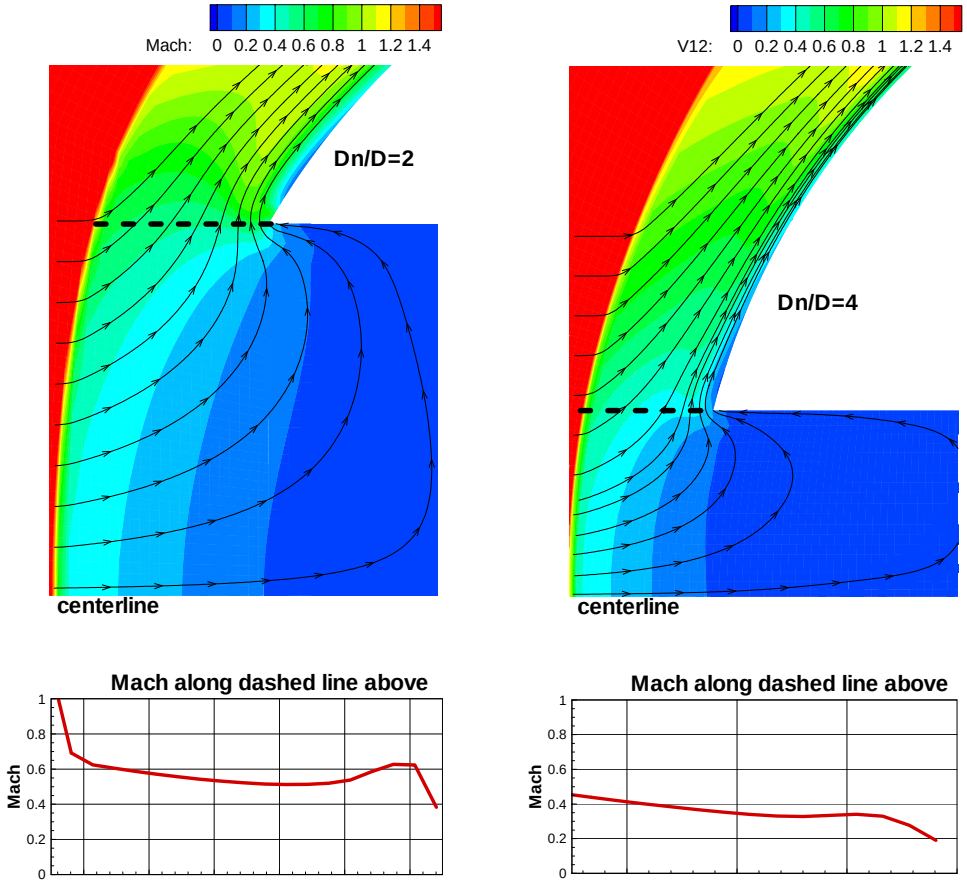

Figure 18. Radial convection currents near cavity mouth for nose-to-cavity diameter ratios of 2 and 4

E. Discussion of Onset of Self-sustained Oscillations

A plausible explanation for the onset of self-sustaining oscillations at sufficient deep cavities is presented. The SMD model results, and laser perturbation experiments by Ladoon and Schneider [Ref. 8], support the idea that the dissipation levels decrease rapidly as cavity depth increases, with all other geometric and flow parameters unchanged. It is suggested that there is a small negative (or reverse) dissipation effect associated with the motion of the bow shock, which leads to the onset of self-sustaining oscillations for deep cavities.

Based on animations of strong oscillatory behavior (refer to Figure 6), there are fundamental differences during the fill and purge phases. During cavity fill there is relatively low pressure and high velocity downstream of the bow shock and the incoming airstream flows into (or impinges) the cavity region without significant radial flow (i.e., the axisymmetric relieving effect is small). The effective radial pressure gradient is reduced by the bow shock's downstream motion. The bow shock also flattens somewhat, perhaps contributing to more uniform fill conditions. In contrast, during cavity purge, there is relatively high pressure and low velocity downstream of the bow shock and the incoming airstream flow contains strong radial currents (i.e., axisymmetric relieving effect is large). The effective radial pressure gradient is increased by the bow shock's upstream motion. Consequently, the

effective force applied by the incoming flow is larger during the cavity inflow phase than during the cavity outflow phase, and this creates a "reverse dissipation."

V. Conclusions

An acoustic analog which represents the freestream-driven behavior of forward-facing cavities in supersonic flow (i.e., Hartmann whistle) has been developed using lumped mechanical elements for mass, stiffness, and dissipation. The dissipation is proposed to be due to baffled-piston type radiation with the bow shock acting as a reflector that reduces dissipation. A CFD flow solver has been used to successfully predict the onset of self-sustained oscillations recently captured experimentally in a Mach 4 quiet tunnel facility.

The sensitivity of pressure amplification within the cavity to disturbance frequency and amplitude, cavity depth, freestream Mach number, and nose-to-cavity diameter have been evaluated using the CFD solver and SMD model. The SMD adequately captures the sensitivity to disturbance frequency and amplitude, cavity depth, high freestream Mach, and large nose-to-cavity diameter ratio, but fails to accurately represent trends at low Mach number and small nose-to-cavity diameter ratio. The likely sources of the deficiencies are described, and demonstrate the difficulties in applying a linear acoustic model representation to this complex unsteady flow. A plausible explanation is provided for the onset of self-sustaining oscillations.

Acknowledgments

The authors would like to thank Dr. Steven Schneider and Mr. Rodrigo Segura for providing experimental data and Embry-Riddle Aeronautical University (ERAU) for providing Linux cluster supercomputer resources.

References

[1]Hartmann, J., Troll, B., "On a New Method for the Generation of Sound Waves," Phys. Rev., Vol. 20, 1922, 719-727.

[2]Engblom, W., Goldstein, D., Ladoon, D., and Schneider, S., "Fluid Dynamics of Hypersonic Forward-Facing Cavity Flow," *AIAA Journal of Spacecraft and Rockets*, July-Aug. 1997, Vol. 34, No. 4, pp. 437-444.

[3]Engblom, W., Goldstein, D., "Nose-tip Surface Heat Reduction Mechanism," *AIAA Journal of Thermophysics and Heat Transfer*, Oct-Dec 1996, Vol. 10, No. 4, pp. 598-606.

[4]Silton, S., Goldstein, D., "Use of an axial nose-tip cavity for delaying ablation onset in hypersonic flow," *Journal of Fluid Mechanics*, 2005, Vol. 528, pp. 297-321.

[5]Juliano, T., Segura, R., et al, "Starting Issues and Forward-Facing Cavity Resonance in a Hypersonic Quiet Tunnel," AIAA 2008-3735.

[6]Engblom, W., Fletcher, B., and Georgiadis, N., "Validation of Conjugate Heat Transfer Capability for Water-Cooled High-Speed Flows," AIAA-2007-4392.

[6]Morse, P., Ingard, U., Theoretical Acoustics, Princeton Univ. Press, Princeton, NJ, 1986, pp. 482-483.

[7]Engblom, W., Goldstein, D., "Fluid Dynamics of Unsteady Cavity Flow," IAT report 0121, Nov. 1996.

[8]Ladoon, D., Schneider, S., "Laser-Induced Resonance in a Forward-Facing Cavity at Mach 4," AIAA 1997-339.